



OPEN

Exosite inhibition of ADAMTS-5 by a glycoconjugated arylsulfonamide

Salvatore Santamaria¹✉, Doretta Cuffaro², Elisa Nuti²✉, Lidia Ciccone², Tiziano Tuccinardi², Francesca Liva², Felicia D'Andrea², Rens de Groot^{1,3}, Armando Rossello² & Josefin Ahnström¹

ADAMTS-5 is a major protease involved in the turnover of proteoglycans such as aggrecan and versican. Dysregulated aggrecanase activity of ADAMTS-5 has been directly linked to the etiology of osteoarthritis (OA). For this reason, ADAMTS-5 is a pharmaceutical target for the treatment of OA. ADAMTS-5 shares high structural and functional similarities with ADAMTS-4, which makes the design of selective inhibitors particularly challenging. Here we exploited the ADAMTS-5 binding capacity of β -*N*-acetyl-D-glucosamine to design a new class of sugar-based arylsulfonamides. Our most promising compound, 4b, is a non-zinc binding ADAMTS-5 inhibitor which showed high selectivity over ADAMTS-4. Docking calculations combined with molecular dynamics simulations demonstrated that 4b is a cross-domain inhibitor that targets the interface of the metalloproteinase and disintegrin-like domains. Furthermore, the interaction between 4b and the ADAMTS-5 Dis domain is mediated by hydrogen bonds between the sugar moiety and two lysine residues (K532 and K533). Targeted mutagenesis of these two residues confirmed their importance both for versicanase activity and inhibitor binding. This positively-charged cluster of ADAMTS-5 represents a previously unknown substrate-binding site (exosite) which is critical for substrate recognition and can therefore be targeted for the development of selective ADAMTS-5 inhibitors.

A Disintegrin And Metalloproteinase with Thrombospondin motif (ADAMTS)-5 (aggrecanase-2) is a metalloproteinase that is important for the proteolytic regulation of the large-aggregating proteoglycans (PGs) aggrecan and versican. These two PGs are responsible for the viscoelastic properties of cartilaginous tissues and large blood vessels, respectively, which are mediated by the glycosaminoglycan (GAG) chains attached to their protein core^{1,2}. Dysregulated proteolysis of aggrecan leads to loss of mechanical resilience of cartilage and is therefore a landmark of degenerative pathologies such as osteoarthritis (OA)^{2,3}. In vitro, ADAMTS-5 is the most potent protease against both aggrecan and versican, being 20–30 fold more active than ADAMTS-4 (aggrecanase-1), its closest family member^{4,5}. In contrast to *Adamts-4* null mice⁶, *Adamts-5* null mice are protected from cartilage degradation in mechanical and inflammatory OA models^{7,8}. Furthermore, inhibitory antibodies against ADAMTS-5 can block aggrecan degradation both in ex vivo and in vivo in models of OA^{9,10}. From a pharmaceutical perspective, ADAMTS-5 is therefore a promising therapeutic target for the treatment of degenerative joint diseases such as OA. However, like many members of the ADAMTS family, ADAMTS-5 is a challenging protein to study due to low expression levels, association with the extracellular matrix, complex post-translational regulation and amenability to (auto)proteolytic degradation^{4,11}. It is comprised of a pro-domain (Pro), a metalloproteinase (Mp) domain, a disintegrin-like (Dis) domain, a central thrombospondin-like (Ts) motif, a cysteine-rich (CysR) domain, a spacer (Sp) domain and a C-terminal Ts motif. The Mp domain contains a conserved sequence (HEIGHLLGLSH) where three histidine residues coordinate the zinc ion that is necessary for catalysis. To date, only the crystal structures of the Mp and Dis domains have been solved^{12,13}. The lack of structural data for the C-terminal domains has hampered the development of small molecule inhibitors targeting these regions. As a result, all reported ADAMTS-5 synthetic inhibitors act through chelation of the catalytic zinc ion in the Mp domain. The vast majority of current inhibitors contain a zinc-binding group (ZBG), such as hydroxamate or carboxylate¹⁴. Common drawbacks exhibited by such inhibitors include poor selectivity due to cross-inhibition of other zinc-containing metalloproteinases, high rate of metabolic conversion and poor bioavailability after oral administration. Combined, these are all factors that have limited pre-clinical applications¹⁴. A strategy to

¹Department of Immunology and Inflammation, Imperial College London, Du Cane Road, London W12 0NN, UK. ²Department of Pharmacy, University of Pisa, via Bonanno 6, 56126 Pisa, Italy. ³Institute of Cardiovascular Science, University College London, 51 Chenies Mews, London WC1E 6HX, UK. ✉email: s.santamaria@imperial.ac.uk; elisa.nuti@unipi.it

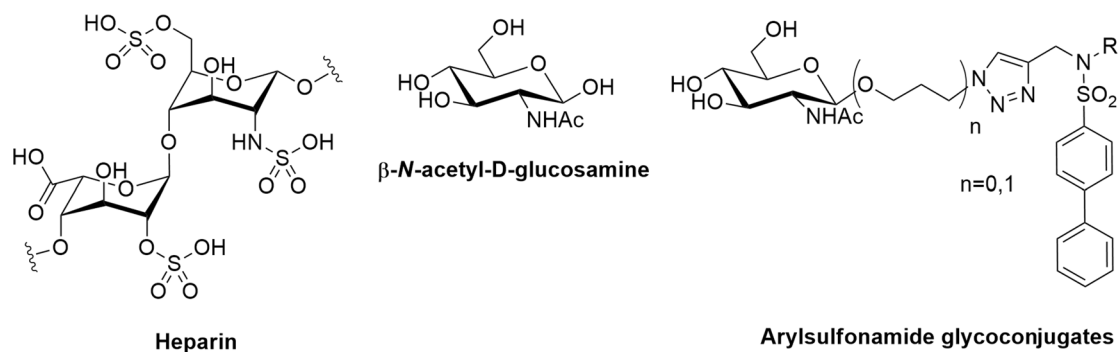


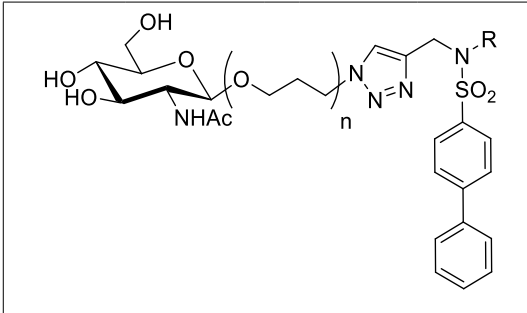
Figure 1. Comparison between heparin and the glycoconjugates analyzed in this study. R represents either a ZBG or an aliphatic moiety.

circumvent these drawbacks would be to target specific amino acid residues in the ancillary domains that are necessary for recognition and binding of PGs (i.e. so-called exosites). We have recently identified two such exosites in the ADAMTS-5 Sp domain (residues 739–744 and 837–844)⁵. These regions are essential for proteolysis of both aggrecan and versican and lie in loops which are hypervariable within the ADAMTS family⁵, thus offering a target for the development of selective inhibitors. However, exposed loops on metalloproteinases can be more easily targeted by antibodies than by small molecules¹⁵, while small molecule inhibitors tend to bind hydrophobic crevices¹⁶. GAGs represent a potential third avenue to exosite inhibition. For example, heparin, a naturally occurring GAG, inhibits the proteoglycanase activity of ADAMTS-5 by binding to the Sp and CysR domains^{4,11,17}. However, due to its anticoagulant properties and associated side effects, such as bleeding¹⁸ and thrombocytopenia¹⁹, heparin itself is not suitable as a therapeutic inhibitor. In heparin, the most common disaccharide unit is composed of a 2-*O*-sulfated iduronic acid and 6-*O*-sulfated, *N*-sulfated β -*N*-acetyl-D-glucosamine (GlcNAc), which we here have exploited for the development of an ADAMTS-5 inhibitor. For this purpose, we probed ADAMTS-5 with a small library of GAG-mimetic molecules, containing the GlcNAc moiety (Fig. 1). Starting from our previously described zinc-chelating inhibitors, with no selectivity for ADAMTS-5 *versus* ADAMTS-4²⁰, we successfully identified an ADAMTS-5-selective glycoconjugate, devoid of a ZBG with activity in the low micromolar range. Furthermore, we show that the GlcNAc moiety of the inhibitor binds to a cluster of positively-charged residues in the ADAMTS-5 Dis domain. Through mutagenesis and biochemical characterization, we also show that these residues compose a novel exosite which is amenable to selective inhibition.

Results

Development of an ADAMTS-5 exosite inhibitor. The primary aim of this study was to identify a selective ADAMTS-5 exosite inhibitor. Exosites are located away from the active site and therefore most of them do not bind small synthetic peptides that are used in the standard Quenched-Fluorescent (QF) peptide cleavage assays⁹. Therefore, to accurately measure inhibition by *exosite* inhibitors, we used our novel ELISA-based assay that employs V1-5GAG, a truncated versican V1 variant, as a substrate. This contains all the binding sites for efficient cleavage by ADAMTS-5 and allows precise kinetic quantification of inhibition^{5,21}.

To develop ADAMTS-5 exosite inhibitors, we started with heparin mimetics (GlcNAc based) fused to an arylsulfonamide scaffold containing a weak ZBG (carboxylic acid)²⁰. In the second stage, we removed the ZBG to increase selectivity. We first performed a small structure–activity relationship (SAR) study with these glycoconjugated arylsulfonamides having either the GlcNAc directly attached to the arylsulfonamido group or via a *n*-propyloxy linker (Table 1). Our previously described inhibitors, compounds **1** and **2**²⁰, inhibited ADAMTS-5 and ADAMTS-4 to a similar level, with half maximal inhibitory concentration (IC₅₀) values in the micromolar range (Table 1). Replacement of the carboxylate with a benzyl ester completely abolished inhibitory activity in both series (compounds **3a** and **4a**), likely due to steric hindrance. Importantly, replacement of the carboxylic acid ZBG with a *sec*-butyl group to generate compound **4b** improved ADAMTS-5 inhibition against V1-5GAG approximately fivefold and, at the same time, abolished ADAMTS-4 inhibition (Fig. 2A; Table 1). This is a remarkable increase in selectivity, in light of the homology and the functional overlap between these two proteases. The presence of an *n*-propyloxy link between the sugar and the arylsulfonamide was essential for inhibition of ADAMTS-5 versicanase activity as shown by the ~13-fold reduction in inhibition when the sugar was directly linked to the sulfonamide scaffold as in compound **3b** (Table 1). Interestingly, when tested in a QF peptide cleavage assay (Table 2), **4b** did not inhibit ADAMTS-5 peptidolytic activity, suggesting that this compound may target an exosite. To understand the binding mode of the inhibitor, we performed systematic modifications of **4b** (Table 2, inhibition curves are reported in Fig. 2A and Supplementary information Fig. S1). Replacement of GlcNAc either with D-galactosamine (GalNAc) (compound **5b**), or a benzoyl group (compound **6**) abolished inhibitory activity, suggesting not only a direct interaction of the GlcNAc with ADAMTS-5, but also that the position of the hydroxyl groups in the sugar moiety is essential for inhibition. The introduction of a benzyloxyphenyl in the arylsulfonamide moiety was reported to greatly improve the inhibitory activity of arylsulfonamide hydroxamates against ADAMTS-5²². Compounds containing this modification (**4c** and **4d**) showed a severe reduction in inhibitory activity which was also associated with a decreased selectivity over ADAMTS-4 (Table 2), suggesting a different mode of interaction for the glycoconjugates.



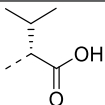
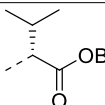
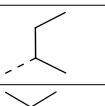
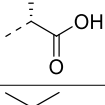
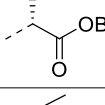
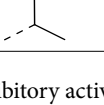
Compound	R	n	IC ₅₀ (μM)	
			ADAMTS-4	ADAMTS-5
1		0	40 ± 5	68 ± 6.5
3a		0	NI	NI
3b		0	50 ± 16	120 ± 20
2		1	51 ± 7.9	44 ± 8.9
4a		1	NI	NI
4b		1	NI	9.4 ± 2.8

Table 1. Inhibitory activities of glycoconjugates 1, 2, 3a, 3b, 4a and 4b against ADAMTS-4 and -5. The inhibition of proteolysis was measured using the protein substrate V1-5GAG. NI, not inhibiting at 50 μM (< 10% inhibition compared with the DMSO controls). Values are presented as mean ± SEM (n = 3).

Importantly, the inhibition of ADAMTS-5 by **4b** was confirmed using aggrecan as a substrate. Compound **4b** effectively inhibited aggrecan proteolysis at Glu392↓Ala393 (Fig. 2B) (Supplementary information Fig. S2), the cleavage site which is most detrimental for cartilage integrity²³. Approximately 80% ADAMTS-5 inhibition was observed at 10 μM. In contrast, the analogue compound devoid of the sugar moiety, **6**, had no effect upon aggrecan cleavage (Fig. 2B). The GalNAc-derivative **5b**, epimer at C-4 of **4b**, induced a modest increase in aggrecanase activity, thus further demonstrating the importance of the hydroxyl configuration for the observed inhibitory potential. These results confirmed that **4b** is suitable for further development as a potential disease-modifying OA agent.

Binding mode of compound 4b. To further probe the interaction of **4b** with ADAMTS-5, we compared its inhibitory activity against ADAMTS-5 MDTCS (lacking the C-terminal TS motif but retaining full versicanase activity)⁴, and its variant consisting only of the Mp and Dis domains (ADAMTS-5 MD), the minimal variant endowed with detectable proteoglycanase activity (Fig. 3A,B)¹¹. As previously reported⁵, deletion of the C-terminal ancillary domains reduced ADAMTS-5 versicanase activity by approximately 730-fold (k_{cat}/K_m : $(34.3 \pm 0.43) \times 10^5 \text{ M}^{-1} \text{ s}^{-1}$ for ADAMTS-5 MDTCS *versus* $(0.14 \pm 0.03) \times 10^5 \text{ M}^{-1} \text{ s}^{-1}$ for ADAMTS-5 MD, $p < 0.001$). In the presence of 100 μM of compound **4b**, ADAMTS-5 MDTCS and MD cleaved V1-5GAG with k_{cat}/K_m values of $(10.0 \pm 0.30) \times 10^5 \text{ M}^{-1} \text{ s}^{-1}$ and $(0.047 \pm 0.010) \times 10^5 \text{ M}^{-1} \text{ s}^{-1}$, respectively. This corresponds to a 71% and 66% reduction in activity for the MDTCS and MD variants, respectively ($p < 0.001$ for both compared to their controls containing equal amounts v/v of dimethyl sulfoxide, DMSO). The similar extent of inhibition exerted by compound **4b** on the two variants confirms that this inhibitor binds to the Mp/Dis domains.

Since compound **4b** is devoid of an obvious ZBG and does not have any effect on the ADAMTS-5 peptidolytic activity while still inhibiting its proteoglycanase activity (Table 2), we hypothesized that it does not interact with the ADAMTS-5 catalytic zinc. To test this, we performed QF peptide cleavage assays at increasing concentrations

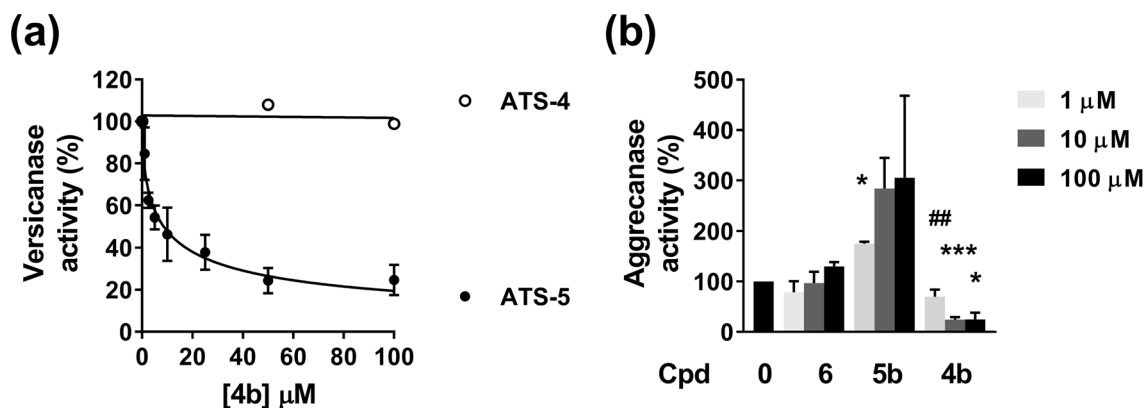
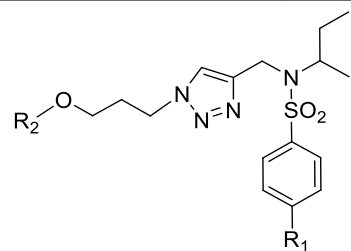


Figure 2. Inhibitory activity of compound **4b**. **(A)** Inhibition of versicanase activity. ADAMTS-4 (5.5 nM) and -5 (0.4 nM) were incubated either with compound **4b** or DMSO for 2 h at 37 °C before addition of V1-5GAG (50 nM). At each time point, reactions were stopped by addition of EDTA and ADAMTS-generated versican fragments (versikine) quantified by sandwich ELISA. The relative versicanase activity is presented and 100% activity corresponds to that in the presence of DMSO alone. **(B)** Inhibition of ADAMTS-5 aggrecanase activity. Compounds (Cpd) **4b**, **5b** and **6** were incubated with ADAMTS-5 (1 nM) for 2 h at 37 °C before addition of aggrecan (20 μg). Following SDS-PAGE and immunoblot, fragments cleaved at the Glu392↓Ala393 bond were detected by a monoclonal neoepitope antibody recognizing the new C-terminal fragment (anti-ARGSV) and analyzed by densitometric analysis. Data are presented as mean ± SEM (n = 4). * $p < 0.05$ and *** $p < 0.001$, compared to DMSO controls; ## $p < 0.01$, compared to the same concentration of compound **6** (Mann–Whitney test).

of GM6001 (Ilomostat, 0–800 nM), a known zinc-binder and broad-spectrum metalloproteinase inhibitor^{22,24}, in the presence or absence of 10 μM **4b** (Fig. 3C,D). The inhibitory activity of GM6001 was quantified as an IC_{50} in the presence (IC_{50}^+) and absence (IC_{50}^-) of **4b**. If the IC_{50} of GM6001 was unchanged in the presence of **4b** ($IC_{50}^+/IC_{50}^- \sim 1$) no synergism between the molecules would occur, whereas if the IC_{50} was reduced ($IC_{50}^+/IC_{50}^- < 1$) or increased ($IC_{50}^+/IC_{50}^- > 1$), the interaction would be synergistic or antagonistic, respectively. GM6001 showed a large increase in inhibition in the presence of **4b** ($IC_{50}^+ = 16 \pm 5$ nM/ $IC_{50}^- = 370 \pm 90$ nM; $IC_{50}^+/IC_{50}^- = 0.043$, $p < 0.05$), and therefore acted as a synergistic inhibitor together with **4b**. This confirms that **4b** does not bind the catalytic zinc, but binds close enough to the active site to have a synergistic effect upon GM6001 binding. This is also in agreement with the results using ADAMTS-5 MD (Fig. 3B) which suggested that the interaction site for **4b** is contained within these two domains.

Molecular docking and molecular dynamics simulations. To investigate how compound **4b** interacts with ADAMTS-5, docking calculations combined with molecular dynamics (MD) simulations were carried out. The compound was docked into the Mp and Dis domains of ADAMTS-5 (PDB code: 2RJQ) complexed with GM6001 using AUTODOCK 4.2 software. Two hundred docking poses were generated and then clustered by applying a root-mean-square deviation (RMSD) of 6.0 Å. The cluster analysis suggested three possible dispositions for **4b** (Supplementary information Fig. S3). Therefore, a representative docking pose belonging to each of the three cluster of poses (C1–C3) was subjected to a 103 ns MD simulation with explicit water molecules, followed by analysis of the three binding modes through the molecular mechanics and Poisson Boltzmann surface area (MM-PBSA) method (Supplementary Information Fig. S4 and Table S1). The results obtained from these analyses suggested the MD-refined C1 pose as the most reliable binding disposition of **4b** within ADAMTS-5. As shown in Fig. 4A (available as Supplementary File 1), the sugar portion of the molecule interacts with the Dis domain of ADAMTS-5, whereas the remaining parts the molecule interacts with the Mp domain. Figure 4B shows the main interactions of **4b** with ADAMTS-5. The biphenyl fragment is water-exposed and shows lipophilic interactions with H374. One of the two oxygen atoms of the sulfonamide moiety forms an hydrogen (H)-bond with the hydroxyl group of S375 whereas the triazole ring shows lipophilic interactions with the indole ring of GM6001. Thus, the results obtained from the docking experiments provide a mechanistic rationale for the synergistic effect observed in the QF peptide cleavage assay. Finally, a particularly important finding was that the GlcNAc moiety showed H-bond interactions with ADAMTS-5 Dis domain residues K532 and K533. The length of the linker appears to be critical in positioning the GlcNAc group at the right distance from the Dis domain, as also shown by the reduced inhibitory potency and selectivity exhibited by compound **3b**, where the sugar is directly linked to the sulfonamide group (Table 1).

The same procedure used above was applied to analyze the hypothetical binding mode of compound **4b** in the absence of GM6001. The docking calculations obtained by means of AUTODOCK 4.2 suggested two possible dispositions for **4b**, CL1 and CL2 (Supplementary Information Fig. S5). A representative pose belonging to each of the two cluster of poses (CL1–CL2) was subjected to a 103 ns MD simulation with explicit water molecules, followed by analysis of the two binding modes through the MM-PBSA method as described above. The results generated were unable to highlight any preference between the two ligand orientations as they differed only about 2 kcal/mol in terms of energy (Table S2). The two orientations shared the disposition of the biphenyl sulfonamide fragment that was inserted inside the S1' cavity with the formation of two H-bonds with the nitrogen



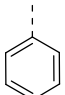
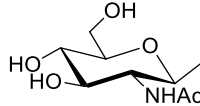
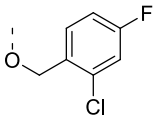
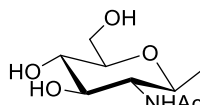
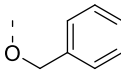
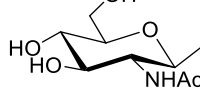
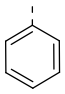
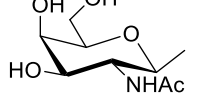
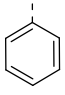
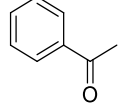
Compound	R ₁	R ₂	IC ₅₀ (μM) QF peptide		IC ₅₀ (μM) V1-5GAG	
			ATS4	ATS5	ATS4	ATS5
4b			NI ^a	NI ^a	NI ^b	9.4 ± 2.8
4c			NI ^a	57 ± 10	90 ± 44	62 ± 12
4d			NI ^a	NI	180 ± 50	90 ± 23
5b			NI ^a	NI ^a	30% inhibition at 100 μM	NI ^b
6			NI ^a	NI ^a	NI ^b	NI ^b

Table 2. Inhibitory activities of 4b and its derivatives, 4c, 4d, 5b and 6, against ADAMTS-4 and -5. The inhibition of proteolysis was measured using either a short, 12-residue, peptide substrate (QF-peptide) or the protein substrate V1-5GAG. Values are presented as mean ± SEM (n = 3). ATS4, ADAMTS-4; ATS5, ADAMTS-5. NI^a, not inhibiting at 50 μM. NI^b, not inhibiting at 100 μM (< 10% inhibition compared with the DMSO controls).

backbone of G379 and L380. In the first orientation, CL1, the rest of the molecule is directed towards the Dis domain forming H-bonds with L443 through the triazole ring and with K532 and K533 through the GlcNAc portion of the ligand (Supplementary Information Fig. S5A). In the second hypothetical binding orientation of 4b, CL2, the ligand is directed towards the S3 portion of the protein and forms an H-bond with D383 through the GlcNAc moiety (Supplementary Information Fig. S5B).

In order to investigate the potential effect of the substitution of the biphenyl with a benzyloxyphenyl fragment, the interaction of compound 4c was analyzed and compared to that of 4b. As shown in Supplementary Information Fig. S6, compound 4c maintained the disposition of 4b with the formation of the two H-bonds with K532 and K533. However, the presence of the 2-chloro-4-fluorobenzyl group caused a small shift of the sulfonamide group towards the protein that determined the loss of the H-bond with S375, thus potentially explaining the 6-fold reduction in inhibitory properties of this compound.

Identification of an exosite in the ADAMTS-5 Dis domain. Our experimental and in silico results both suggested that 4b functions as a cross-domain exosite inhibitor. They also suggested that residues K532 and K533 may compose an undescribed exosite in the ADAMTS-5 Dis domain. To further investigate the importance of K532 and K533 as a potential exosite for versican cleavage and inhibition by compound 4b, we substituted both residues either to alanine (variant K532A/K533A) or glutamine (variant K532Q/K533Q) in ADAMTS-5 MDTCS. An amino acid sequence alignment of the Dis domains showed that ADAMTS-4 retains a lysine residue at position 532 but presents a histidine residue at position 533 (Fig. 4C). Since compound 4b is selective for ADAMTS-5 over ADAMTS-4, we also substituted K533 to histidine (K533H), to determine how important this residue is for inhibitor selectivity. ADAMTS-5 K533A was generated to assess the overall importance of K533 for substrate recognition and protein stability. All variants were transiently expressed in HEK293T cells. Western blot analysis of conditioned media demonstrated that all mutants were expressed and secreted at similar levels

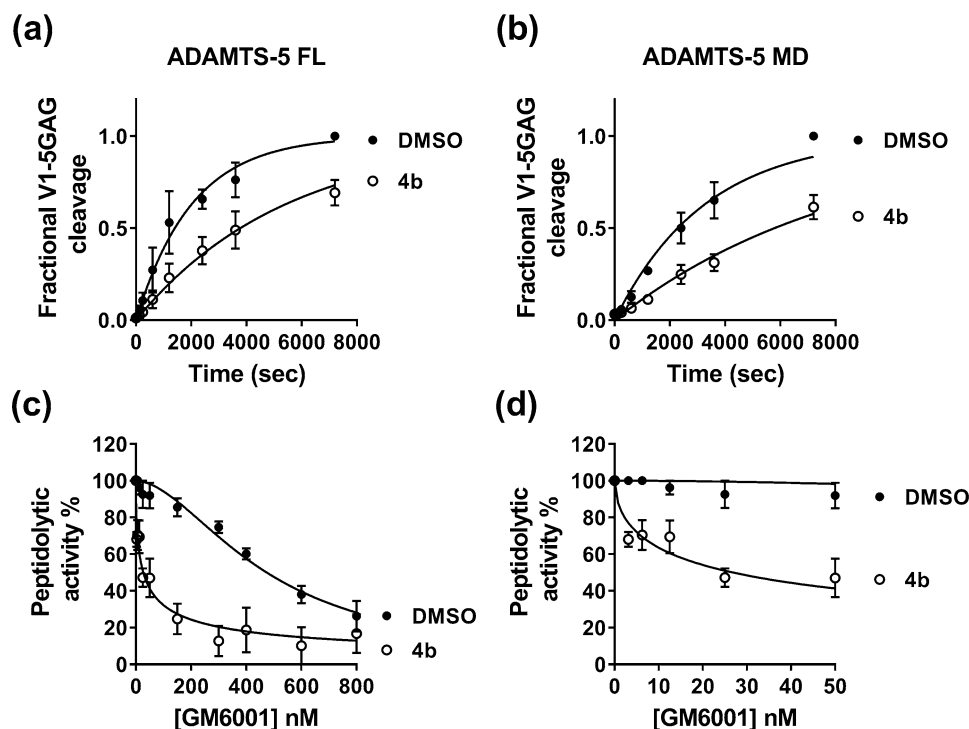


Figure 3. Compound **4b** binds to the ADAMTS-5 Mp/Dis domains in the presence of GM6001. (A, B) Compound **4b** inhibits versicanase activity of both full-length (FL) ADAMTS-5 and its variant containing only the Mp/Dis domains (ADAMTS-5 MD). Compound **4b** (100 μ M) or DMSO was incubated either with ADAMTS-5 FL (0.2 nM, A) or ADAMTS-5 MD (26 nM, B) for 2 h at 37 $^{\circ}$ C before addition of V1-5GAG (50 nM). At each time point, reactions were stopped by addition of EDTA and versikine fragments quantified by sandwich ELISA as reported in the Methods section. In the DMSO control, complete proteolysis was achieved after 7200 s. (C, D) Inhibition of ADAMTS-5 peptidolytic activity by the active-site inhibitor GM6001 in the presence of compound **4b**. ADAMTS-5 MDTCS was incubated with active-site inhibitor GM6001 (0–800 nM) either in the presence of DMSO or compound **4b** (10 μ M) for 2 h at 37 $^{\circ}$ C before addition of QF peptide. The synergistic effect exerted by compound **4b** is more evident at low concentrations of GM6001 (panel D). The relative peptidolytic activity is presented and 100% activity corresponds to that in the presence of DMSO alone. Data are presented as mean \pm SEM ($n=3$).

to that of wild-type ADAMTS-5 (Supplementary information Fig. S7A). Following purification (Supplementary information Fig. S7B), these variants were tested in the versican digestion assay (Fig. 4D; Table 3). Interestingly, replacement of the two contiguous lysine residues resulted in a significant reduction in versicanase activity, suggesting that these residues are necessary for recognition and proteolysis of PGs. Critically, compound **4b** was unable to inhibit the versicanase activity of K532A/K533A (Fig. 4E). These results confirm our *in silico* model of the interactions between compound **4b** and ADAMTS-5 in the presence of GM6001 (Fig. 4A,B). They also show that K532/K533 are acting as an exosite for PG binding and recognition in ADAMTS-5 which is blocked when ADAMTS-5 is bound to compound **4b**. Moreover, they also favor a binding mode in the absence of GM6001 consistent with pose CL1 (Supplementary Information Fig. S5A) where the main interactions with the ADAMTS-5 Dis domain are preserved. Replacement of K533 either to alanine (to abolish the positive charge on side chain) or histidine (as in ADAMTS-4) resulted only in a modest reduction in versicanase activity. Compound **4b** did not show inhibitory activity against the K533H variant (Fig. 4E), thus demonstrating that binding of the inhibitor to Lys533 in ADAMTS-5 creates the desired selectivity against ADAMTS-4.

Discussion

Cumulative evidence from the last 20 years has recognized ADAMTS-5 as a target for OA. Currently, three clinical trials (ID: NCT03595618, NCT03583346 and NCT03224702) are under way to assess the efficacy of ADAMTS-5 inhibitors as OA therapeutics. These involve a small molecule containing a ZBG and a monoclonal antibody²⁵. However, many inhibitors have failed at the preclinical stage²⁵, a major reason being the lack of adequate selectivity. To create a break-through, we aimed to alter the principle behind the inhibition from active site inhibition to exosite inhibition. This was made possible by our kinetic assay, using versican instead of peptides as a substrate⁹.

Our inhibitor design strategy involved conjugating GlcNAc to a ZBG-arylsulfonamide scaffold, followed by removal of the ZBG. This strategy diverges from the traditional approach where ZBGs are attached to an S1' binding moiety²⁶. We confirmed that our lead compound **4b** does not bind to the active site zinc, as shown by the lack of inhibition of QF peptide cleavage, as well as its synergism with the zinc-chelating broad-spectrum

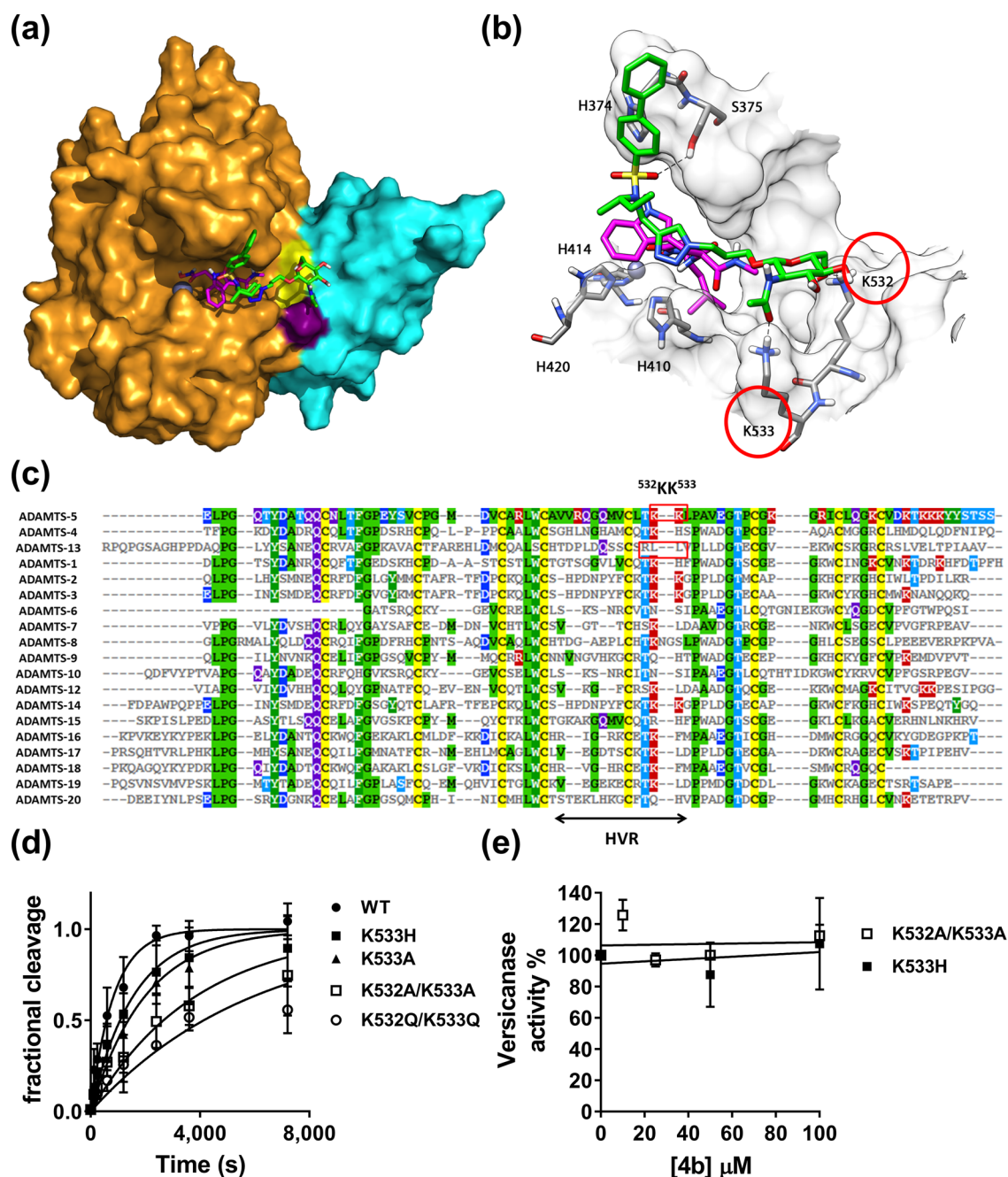


Figure 4. Compound **4b** binds to an exosite in the ADAMTS-5 Dis domain. **(A, B)** Minimized average structure of compound **4b** bound to the ADAMTS-5-GM6001 complex, derived from the last 100 ns of MD simulation. **(A)** Protein surface. **4b** is shown in green, GM6001 is in pink, ADAMTS-5 Mp domain in gold, the Dis domain in light blue, the active site zinc as a grey sphere. Exosite residues K532 and K533 are colored in yellow and purple, respectively. **(B)** Protein residues directly interacting with compound **4b**. H-bonds are represented as black dashed lines. **(C)** Amino acid sequence alignment of the Dis domain of all ADAMTS family members. Known exosites are boxed and the poorly conserved region (HVR, hypervariable region) is indicated. Conserved residues are indicated by the same color code. **(D)** Time course experiments for cleavage of 50 nM V1-5GAG by ADAMTS-5 MDTCS variants. Enzyme (0.4 nM) was incubated with 50 nM substrate. At the indicated time points, an aliquot was taken, stopped with EDTA and cleavage products measured by sandwich ELISA as described in the Methods section. The solid lines represent a nonlinear regression fit of the data. The data are presented as average \pm SEM; n = 3–4. **(E)** Inhibition of ADAMTS-5 MDTCS variants by compound **4b**. ADAMTS-5 K533H and K532A/K533A (0.82 nM) were incubated either with compound **4b** or DMSO for 2 h at 37 °C before addition of V1-5GAG (50 nM). At each time point, reactions were stopped by addition of EDTA and cleavage fragments quantified by sandwich ELISA. The relative versicanase activity is presented and 100% activity corresponds to that in the presence of DMSO alone. The data are presented as average \pm SEM; n = 3.

ADAMTS-5 variant	k_{cat}/K_m $10^5 \text{ M}^{-1} \text{ s}^{-1}$	Fold reduction
MDTCS	32.3 ± 7.64	–
K532A/K533A	6.75 ± 2.22*	4.8
K532Q/K533Q	4.01 ± 0.49*	8.0
K533A	12.5 ± 2.75*	2.6
K533H	15.6 ± 4.17	2.1

Table 3. Kinetic parameters for proteolysis of V1-5GAG by ADAMTS-5 variants. Values were determined by time course experiments at 50 nM V1-5GAG substrate concentration. Results are expressed as mean ± SEM. * $p < 0.05$, compared to ADAMTS-5 MDTCS according to Mann–Whitney tests ($n = 3$).

metalloproteinase inhibitor GM6001. Replacement of the GlcNAc either with a benzoyl group or a GalNAc (Table 2) abolished inhibitory activity, suggesting a direct interaction of the GlcNAc with ADAMTS-5. To our knowledge, a similar role of an amino sugar moiety has not been reported previously for metzincin inhibitors. Instead, the addition of a carbohydrate group has been envisaged as a way to increase the hydrophilicity of metalloproteinase inhibitors and thus enhance their oral availability, without affecting their inhibitory activity^{20,27–30}. Using a combination of kinetic and in silico studies, we demonstrated that **4b** is an exosite cross-domain inhibitor, acting by an unprecedented mechanism where the S1' pocket is occupied by the arylsulfonamide portion, whereas the sugar moiety interacts with the exosite in the Dis domain. Overall, the binding of **4b** may have two consequences: (1) to occlude access of PGs to the active site; (2) “freezing” the flexibility between the Mp and Dis domains in a way similar to the inhibitory antibody described by Larkin et al.¹⁰.

In contrast to what their names suggest, the Dis domains of ADAMTS family proteases do not share homology with disintegrins, a family of proteins from viper venoms. Instead, they are topologically related to a region in the CysR domains of P-III snake venom metalloproteinases which are involved in binding to platelet integrin receptors^{12,13,31–33}. In ADAMTS-5, the Dis domain lacks any integrin binding sequence and does also not interact with integrins¹³. It has a unique fold of two α -helices, two β -sheets, and several loops throughout the domain and is connected to the Mp domain by a flexible linker that is 9 amino acids long¹³. The Dis domain lies on the prime side of the active site, where it shields the S1' pocket and, to a lesser extent, the S3' pocket from solvent¹³. Previous studies have shown that the isolated ADAMTS-5 Mp domain alone is unable to cleave PGs^{11,21}. Its proteoglycanase activity is partially restored when the Dis domain is added (ADAMTS-5 MD), although addition of further C-terminal ancillary domains is necessary for full proteoglycanase activity^{4,5}. The same lack of proteolytic activity of the isolated Mp domain in the absence of the Dis domain, has been observed for several other ADAMTS family members, such as ADAMTS-1³⁴, -4³⁵, -9³⁶, and -13^{37,38}. Together, these results suggest that the Dis domain may be involved in substrate recognition for all five mentioned ADAMTS members.

The GlcNAc group of inhibitor **4b** interacts with residues K532 and K533 in the Dis domain where they constitute a previously undescribed exosite. These two residues lie adjacent to the active site cleft, at a distance of 17–18 Å from the active site zinc, in a region poorly conserved (hypervariable) amongst the ADAMTS family of proteases (Fig. 4C). The ADAMTS-5 Dis exosite partially overlaps with an exosite in ADAMTS-13 (residues R349, L350G and V352G)³⁹. However, the distance between the Dis exosite and the zinc is higher in ADAMTS-13 (~26 Å), possibly to adapt to its specific substrate, von Willebrand factor³⁹. Moreover, the ADAMTS-5 exosite is more positively-charged, suggesting that the interaction with PGs involves more electrostatic than hydrophobic interactions. This hypothesis is supported by the presence of a lysine-rich sequence (⁷³⁹NKKSKG⁷⁴⁴) in the ADAMTS-5 Sp domain which has been suggested to bind heparin¹⁷ and PGs⁵, suggesting similarities between the amino acid composition of the exosites present in the Sp and Dis domains. Semisynthetic polysaccharides such as pentosan polysulfate have also been shown to bind to ADAMTS-5 Mp/Dis through electrostatic interactions¹⁷. Kinetic analysis revealed a 5–8-fold reduction in catalytic efficiency when both K532 and K533 were mutated, thus showing their importance for efficient substrate cleavage. However, this effect is modest compared with that observed after substitutions of the β 1– β 2 and β 9– β 10 loops in the Sp domain (residues 739–744 and 837–844, respectively), which caused a 30–40 fold reduction in versicanase activity, compared to wild-type ADAMTS-5⁵. It is therefore likely that the contact between the Dis exosite and PGs follows an initial binding of the PGs to the ADAMTS-5 Sp domain⁵. Other studies have also suggested the functional importance of the Dis domain. For example, the endogenous inhibitor of ADAMTS-5, Tissue Inhibitor of Metalloproteinase (TIMP)-3, interacts with the Dis domain^{9,40} and monoclonal antibodies, inhibiting ADAMTS-5 function, have also been reported that target this domain^{9,10}. However, to date compound **4b** is the only example of a small molecule binding to the Dis domain. Further optimization of this cross-domain sugar-based exosite inhibitor could lead to the development of a novel class of OA therapeutics with increased selectivity and bioavailability.

Methods

Protein expression and purification. The constructs coding for human ADAMTS-4 and -5 with a C-terminal FLAG tag (DYKDDDDK) in pEGFP-N1 vector have been described previously⁵. ADAMTS-4 and -5 variants were expressed in serum-free MEM containing 200 μ g/mL heparin (Sigma) to extract extracellular matrix-bound enzyme, concentrated using a Lab scale TFF system (Merck) and purified using anti-FLAG affinity resin (Cat. n.: A2220, Sigma) as previously described⁵. Briefly, after loading the medium, the column was washed with 1 M NaCl to remove heparin⁴¹, and the bound protein was eluted with 200 μ g/mL FLAG peptide (Cat. n.:

F3290, Sigma). Proteins were separated by SDS-PAGE and analyzed by western blot using an anti-FLAG M2 mouse monoclonal primary antibody (Cat. n.: F1804, Sigma; 1:1000). Purity was assessed by silver-stain. Concentrations of active ADAMTS-4 and -5 and were determined under kinetic equilibrium conditions by active-site titrations with known concentration of TIMP-3 (Bio-Techne, Cat. n.:973-TM-010, Bio-Techne)⁴² using QF peptides as reported in the “QF Peptide Cleavage assays” section. ADAMTS-5 Dis variants were generated using site-directed mutagenesis and confirmed through sequencing. Since it is known that TIMP-3 interacts with the Dis domain of ADAMTS-5^{9,40}, for the results reported in Table 3, total enzyme concentration was measured by optical absorbance at 280 nm using extinction coefficient of 1.220 (E1%, 1 cm) as predicted by the ProtParam Tool (ExPasy).

The versican V1-5GAG plasmid, comprising amino acids 21–694 of V1 with C-terminal C-myc/6 × His tag has been described previously^{5,21}. V1-5GAG was purified using a Ni-sepharose column (GE Healthcare) equilibrated with 3 column volumes (CV) TBS (20 mM Tris–HCl pH 7.4, 150 mM NaCl). Following binding, the column was washed with TBS containing 10 mM imidazole and bound proteins were eluted using a linear gradient (10–300 mM) of imidazole. Eluted fractions containing recombinant proteins were subjected to SDS-PAGE, pooled, concentrated on Amicon Ultra spin columns (100 kDa cut-off) and dialyzed extensively against TBS, before storage at –80 °C. DNA and protein concentrations were measured using a NanoDrop ND-2000 UV–visible spectrophotometer (Thermo Fisher Scientific, Nottingham, UK).

Inhibition assays. All enzyme assays were conducted in TNC-B buffer (50 mM Tris–HCl, pH 7.5, 150 mM NaCl, 10 mM CaCl₂, and 0.02% NaN₃) at 37 °C. To avoid the formation of inhibitor aggregates, the detergent Brij-35 (0.05%) was added to the assay buffer⁴³. No aggregation was visually observed at concentrations up to 2 mM. The inhibitor stock solutions in DMSO (10 mM) were diluted at different concentrations in assay buffer and incubated with ADAMTS-4 or ADAMTS-5 for 2 h at 37 °C. Percent of inhibition was calculated from control reactions containing only DMSO. IC₅₀ values were determined using the formula: $v_i/v_0 = 1/(1 + [I]/IC_{50})$ where v_i is the initial velocity of substrate cleavage in the presence of the inhibitor at concentration [I] and v_0 is the initial velocity in the presence of an equal concentration (v/v) of DMSO.

Versican digestion assays. ADAMTS-5 full-length (FL) (final concentration 0.4 nM), ADAMTS-5 MDTCS (0.4 nM) ADAMTS-5 MD (26 nM) or ADAMTS-4 (5.5 nM) were incubated with different concentrations of inhibitors or DMSO for 2 h at 37 °C in TNC-B buffer before addition of V1-5GAG (50 nM). At different time points (0–20 min), sub-samples were removed and reactions were stopped with EDTA. Maxisorp plates (VWR, Lutterworth, UK) were coated with 5 µg/mL anti-DPEEAE neopeptide antibody (Cat n. PA1-1748A, Life Technologies, Paisley, UK) in carbonate buffer pH 9.6 (16 h, 4 °C). This neopeptide antibody specifically recognizes the N-terminal versican fragment versikine, generated when ADAMTS-5 cleaves versican at the Glu441↓442Ala bond. Washing steps were performed in triplicate with 300 µL phosphate buffered-saline (PBS) containing 0.1% Tween-20 between each step. Plates were blocked with 3% bovine serum albumin (BSA)/PBS for 2 h, at RT. The samples from the digestion experiments were diluted in 3% BSA/PBS and added to the plate (100 µL, 2 h, RT). Bound versikine fragments were detected using anti-G1 monoclonal antibody (Cat n. ab171887, Abcam, Cambridge, UK) (3 µg/mL in 0.5% BSA/PBS, 1.5 h, RT), followed by horseradish peroxidase (HRP)-conjugated anti-mouse antibodies (Cat. N. P044701-2, Agilent Technologies LTD, Cheshire, UK) (2.4 µg/mL, 1 h, RT). The assay was developed by addition of o-phenylenediamine dihydrochloride (OPD, Cat n. 34006, Sigma Aldrich, Gillingham, UK) for 10 min and reactions were stopped with 2 M H₂SO₄. The absorbance was measured at 492 nm using a BioTek Epoch (BioTek, Swindon, UK) plate reader. For each dilution, the amount of neopeptide generated was derived from a standard curve (0–1.56 nM) of V1-5GAG completely digested with ADAMTS-5. Initial velocities were calculated from the concentration of versikine generated as a function of reaction time and IC₅₀ values were determined.

For inhibition studies, initial rates of proteolysis (<20% cleavage) were analyzed between 0 and 20 min. For determination of the specificity constants (k_{cat}/K_m), digestion reactions were allowed to occur to completion (0–2 h). Data were analyzed as previously described⁴⁴.

Aggrecan digestion assays. ADAMTS-5 (5 nM) was incubated with inhibitors or DMSO for 2 h at 37 °C in TNC-B buffer. Aggrecan from bovine articular cartilage (270 nM) (Cat. n.: A1960 Sigma Aldrich, numbering according to Uniprot accession number P13608) was added. After 2 h digestion at 37 °C, the reactions were stopped with EDTA buffer and the samples incubated with 0.1 U/mL of chondroitinase ABC (AMS Biotechnology, Abingdon, UK) and keratanase (endo-beta galactosidase, Cat. n.: G6920, Sigma Aldrich) in deglycosylation buffer (50 mM sodium acetate, 25 mM Tris HCl pH 8.0) for 16 h at 37 °C to remove GAG chains. Samples were analyzed by SDS-PAGE under reducing conditions (5% β-mercaptoethanol) on 4–12% Bis–Tris NuPage Gels (Thermo Fisher) and cleavage products were detected using mouse monoclonal BC-3 antibody which detects aggrecan cleavage at the Glu392↓Ala393 bond (Cat n.: MA316888, Life Technologies). Immobilon Chemiluminescent HRP substrate (Cat. n. IMGDV002, Merck Millipore, Watford, UK) was used for detection. Bands were detected with a Chemidoc Touch Imaging system (Bio-Rad Laboratories Ltd, Hemel Hempstead, UK) and intensities were measured using Image lab software version 5.2.1.

QF peptide cleavage assays. QF peptide cleavage assays were conducted in 96-well black microtiter plates (Scientific Laboratories Supplies Ltd, Wilford, UK) using a Fluostar Omega microplate reader (BMG Labtech, Aylesbury, UK). The activity of ADAMTS-4 (1 nM) and -5 (5 nM) was monitored for 2 h using the fluorescent peptide substrates fluorescein 5(6)-carbonyl-Ala-Glu-Leu-Asn-Gly-Arg-Pro-Ile-Ser-Ile-Ala-Lys-N,N,N₀,N₀-tetramethyl-6-carboxyrhodamine-NH₂ (FAM-AE~LQGRPISIAK-TAMRA, ADAMTS-4) and fluorescein

5(6)-carbonyl-Thr-Glu-Ser-Glu ~ Ser-Arg-Gly-Ala-Ile-Tyr-Lys-Lys-N,N,N0,N0-tetramethyl-6-carboxyrhodamine-NH₂ (FAM-TESE ~ SRGAIYKK-TAMRA, ADAMTS-5) (custom-synthesized by Bachem, Bubendorf, Switzerland) with an excitation wavelength of 485 nm and an emission wavelength of 538 nm. Final substrate concentrations were 1 μM and 40 μM for ADAMTS-4 and -5, respectively. Fluorescence was expressed in relative fluorescence units (RFU) and normalized against a blank containing only buffer and substrate. Emission spectra were recorded at several concentrations of each compound to exclude auto-fluorescence and maximal inhibitor concentrations were selected accordingly.

Dual inhibition studies. Dual inhibitor experiments were performed essentially as before⁴⁵. Briefly, GM6001 (0–800 nM) was incubated with ADAMTS-5 in the presence and absence of a fixed concentration (10 μM) of compound **4b** and QF peptide cleavage assays were run as above. IC₅₀ values were determined in the absence (IC₅₀⁻) and in the presence of **4b** (IC₅₀⁺). In the latter condition, the activity measured in the presence of **4b** and ADAMTS-5 alone was taken as 100%.

Statistics. Data are presented as mean ± SEM of at least three independent experiments and were analyzed by GraphPad Prism Software. Statistical analysis was performed using Mann–Whitney test. *p* < 0.05 was considered significant.

In silico studies. *Binding of 4b to the ADAMTS-5/GM6001 complex.* Molecular modelling. The crystal structure of human ADAMTS-5 Mp/Dis domains (PDB code 2RJQ)¹³ complexed with its reference inhibitor is currently the only reported structure of the joint Mp/Dis domains in ADAMTS-5 and was therefore chosen for our in silico studies. This structure was minimized using AMBER16 software and ff14SB force field at 300 K, after removing all hydrogen atoms. The complex was placed in a rectangular parallelepiped water box, an explicit solvent model for water, TIP3P, was used and the complex was solvated with a 10 Å water cap. Sodium ions were added as counter-ions to neutralize the system. Two steps of minimization were then carried out; in the first stage, we kept the protein fixed with a position restraint of 500 kcal/mol Å² and we solely minimized the positions of the water molecules. In the second stage, we minimized the entire system through 5000 steps of steepest descent followed by conjugate gradient (CG) until a convergence of 0.05 kcal/Å mol. Molecular docking calculations were performed with AUTODOCK 4.2 using the improved force field^{46,47}. Autodock Tools were used to identify the torsion angles in the ligand, add the solvent model and assign the Kollman atomic charges to the protein, while ligand charges were calculated with the Gasteiger method. A grid spacing of 0.375 Å and a distance-dependent function of the dielectric constant were used for the energetic map calculations. Compound **4b** was subjected to a robust docking procedure already used in virtual screening and pose prediction studies^{48–51}. The docked compound was subjected to 200 runs of the AUTODOCK search using the Lamarckian Genetic Algorithm performing 10,000,000 steps of energy evaluation. The number of individuals in the initial population was set to 500 and a maximum of 10,000,000 generations were simulated during each docking run. All other settings were left as their defaults and the best docked conformation was considered. For the modelling of **4b**/GM6001/ADAMTS-5 co-complex, GM6001 was first subjected to the docking procedure as above. The so-obtained ADAMTS-5-GM6001 complex was used for the docking evaluation of compound **4b** by using all parameters described above. The results were then clustered by applying a root-mean-square deviation (RMSD) of 6.0 Å. The clusters with a population of at least 40 poses (corresponding to the 20% of the total poses) were considered. The cluster analysis suggested three possible binding orientations for **4b** (Supplementary information Fig. S3), which were subjected to MD simulations.

MD simulations. All simulations were performed using AMBER, version 16. MD simulations were carried out using the ff14SB force field at 300 K. The complex was placed in a rectangular parallelepiped water box. An explicit solvent model for water, TIP3P, was used, and the complex was solvated with a 20 Å water cap. Sodium ions were added as counter-ions to neutralize the system. Prior to MD simulations, two steps of minimization were carried out using the same procedure described above. Particle mesh Ewald (PME) electrostatics and periodic boundary conditions were used in the simulation. The MD trajectory was run using the minimized structure as the starting conformation. The time step of the simulations was 2.0 fs with a cut-off of 10 Å for the non-bonded interactions, and SHAKE was employed to keep all bonds involving hydrogen atoms rigid. Constant-volume periodic boundary MD was carried out for 3.0 ns, during which the temperature was raised from 0 to 300 K. Then 100 ns of constant pressure periodic boundary MD was carried out at 300 K by using the Monte Carlo barostat with anisotropic pressure scaling for pressure control. All the α carbons of the protein were blocked with a harmonic force constant of 10 kcal/mol Å². General Amber force field (GAFF) parameters were assigned to the ligand, while partial charges were calculated using the AM1-BCC method as implemented in the Antechamber suite of AMBER 16. A representative docking pose belonging to each of the three cluster of poses (C1–C3) was subjected to a 103 ns MD simulation with explicit water molecules. By analyzing the RMSD of the position of compound **4b** during the simulation with respect to the starting pose, we observed an average RMSD of 6.4 and 7.5 Å for C1 and C3. Considering the high degrees of freedom that characterizes **4b**, these two orientations were considered quite stable. On the other hand, the C2 binding mode was highly unstable (average RMSD: 30.4 Å) (Supplementary information Fig. S4) and therefore discarded. The minimized average structure of the ADAMTS-5/GM6001/**4b** complex was modified and used as a starting point for the construction of the ADAMTS-5/**4c** complex (Supplementary information Fig. S6). Then a 103 ns MD simulation with explicit water molecules as reported above and analyzed.

Binding energy evaluation. Relative binding free energy evaluations were performed using AMBER 16. The trajectories extracted from the last 100 ns of each simulation were used for the calculation, for a total of 100 snapshots (at time intervals of 1 ns). Van der Waals, electrostatic and internal interactions were calculated with the SANDER module of AMBER 16, whereas the Poisson – Boltzmann method was employed to estimate polar energies through the molecular mechanics and Poisson Boltzmann surface area (MM-PBSA) module of AMBER 16 as previously reported⁵¹. Gas and water phases were represented using dielectric constants of 1 and 80, respectively, while nonpolar energies were calculated with MOLSURF program. The entropic term was considered as approximately constant in the comparison of the ligand–protein energetic interactions. All three binding modes were further analyzed through MM-PBSA method. This approach averages the contribution of solvation free energy and gas phase energy for snapshots of the ligand–protein complex and the unbound components extracted from MD trajectories. The results of the MM-PBSA analysis suggested pose C1 as the most favorable binding mode, since it showed an interaction energy (Δ PBSA = – 14.7 kcal/mol) that was more than 8 kcal/mol lower than that estimated for the binding mode C2 and C3 (Supplementary information Table S1). The results obtained from these analyses suggested the MD-refined C1 pose as the most reliable binding disposition of **4b** within ADAMTS-5.

Binding of 4b to ADAMTS-5 in the absence of GM6001. The same procedure described above was applied to investigate the binding of **4b** to ADAMTS-5 Mp/Dis domains (PDB code 2RJQ) in the absence of GM6001.

Chemical synthesis. The initially investigated compounds **1** and **2** were prepared as previously reported²⁰. For synthesis of compounds **3a**, **b**, **4a–d**, **5b** and **6** see supplementary information. Nuclear magnetic resonance spectra are reported in Supplementary information Figures S8–S33.

Data availability

Reagents and data presented in this study are available from the corresponding authors upon request.

Received: 29 June 2020; Accepted: 17 December 2020

Published online: 13 January 2021

References

- Kiani, C., Chen, L., Wu, Y. J., Yee, A. J. & Yang, B. B. Structure and function of aggrecan. *Cell Res.* **12**, 19–32 (2002).
- Wight, T. N. A role for proteoglycans in vascular disease. *Matrix Biol.* **71–72**, 396–420 (2018).
- Heinegård, D. & Saxne, T. The role of the cartilage matrix in osteoarthritis. *Nat. Rev. Rheumatol.* **7**, 50–56 (2011).
- Fushimi, K., Troeberg, L., Nakamura, H., Lim, N. H. & Nagase, H. Functional differences of the catalytic and non-catalytic domains in human ADAMTS-4 and ADAMTS-5 in aggrecanolytic activity. *J. Biol. Chem.* **283**, 6706–6716 (2008).
- Santamaria, S. *et al.* Exosites in hypervariable loops of ADAMTS spacer domains control substrate recognition and proteolysis. *Sci. Rep.* **9**, 10914 (2019).
- Glasson, S. S. *et al.* Characterization of and osteoarthritis susceptibility in ADAMTS-4-knockout mice. *Arthritis Rheum.* **50**, 2547–25458 (2004).
- Glasson, S. S. *et al.* Deletion of active ADAMTS5 prevents cartilage degradation in a murine model of osteoarthritis. *Nature* **434**, 644–648 (2005).
- Stanton, H. *et al.* ADAMTS-5 is the major aggrecanase in mouse cartilage in vivo and in vitro. *Nature* **434**, 648–652 (2005).
- Santamaria, S. *et al.* Antibody-based exosite inhibitors of ADAMTS-5 (aggrecanase-2). *Biochem J.* **471**, 391–401 (2015).
- Larkin, J. *et al.* Translational development of an ADAMTS-5 antibody for osteoarthritis disease modification. *Osteoarthr. Cartil.* **23**, 1254–1266 (2015).
- Gendron, C. *et al.* Proteolytic activities of Human ADAMTS-5. Comparative studies with ADAMTS-4. *J. Biol. Chem.* **282**, 18294–18306 (2007).
- Shieh, H. S. *et al.* High resolution crystal structure of the catalytic domain of ADAMTS-5 (aggrecanase-2). *J. Biol. Chem.* **283**, 1501–1507 (2008).
- Mosyak, L. *et al.* Crystal structures of the two major aggrecan degrading enzymes, ADAMTS4 and ADAMTS5. *Protein Sci.* **17**, 16–21 (2008).
- El Bakali, J. *et al.* Inhibition of aggrecanases as a therapeutic strategy in osteoarthritis. *Future Med. Chem.* **6**, 1399–13412 (2014).
- Santamaria, S. & de Groot, R. Monoclonal antibodies against metzincin targets. *Br. J. Pharmacol.* **176**, 52–66 (2019).
- Cheng, A. C. *et al.* Structure-based maximal affinity model predicts small-molecule druggability. *Nat. Biotechnol.* **25**, 71–75 (2007).
- Troeberg, L. *et al.* Calcium pentosan polysulfate is a multifaceted exosite inhibitor of aggrecanases. *FASEB J.* **22**, 3515–3524 (2008).
- Crowther, M. A. & Warkentin, T. E. Bleeding risk and the management of bleeding complications in patients undergoing anticoagulant therapy: focus on new anticoagulant agents. *Blood* **111**, 4871–4879 (2008).
- Warkentin, T. E. *et al.* Heparin-induced thrombocytopenia in patients treated with low-molecular-weight heparin or unfractionated heparin. *N. Engl. J. Med.* **32**, 1330–1335 (1995).
- Nuti, E. *et al.* Sugar-based arylsulfonamide carboxylates as selective and water-soluble matrix metalloproteinase-12 inhibitors. *Chem. Med. Chem.* **11**, 1626–1637 (2016).
- Foulcer, S. J. *et al.* Determinants of versican-V1 proteoglycan processing by the metalloproteinase ADAMTS5. *J. Biol. Chem.* **289**, 27859–27873 (2014).
- Nuti, E. *et al.* Arylsulfonamide inhibitors of aggrecanases as potential therapeutic agents for osteoarthritis: synthesis and biological evaluation. *Eur. J. Med. Chem.* **62**, 379–394 (2013).
- Little, C. B. *et al.* Blocking aggrecanase cleavage in the aggrecan interglobular domain abrogates cartilage erosion and promotes cartilage repair. *J. Clin. Invest.* **117**, 1627–1636 (2007).
- Saghatelian, A., Jessani, N., Joseph, A., Humphrey, M. & Cravatt, B. F. Activity-based probes for the proteomic profiling of metalloproteases. *Proc. Natl. Acad. Sci. U. S. A.* **101**, 10000–10005 (2004).
- Santamaria, S. ADAMTS-5: a difficult teenager turning 20. *Int. J. Exp. Pathol.* <https://doi.org/10.1111/iep.12344> (2020).
- Lanz, J. & Riedl, R. Merging allosteric and active site binding motifs: de novo generation of target selectivity and potency via natural-product-derived fragments. *Chem. Med. Chem.* **10**, 451–454 (2015).

27. Tsukida, T., Inoue, Y., Kondo, H., Yoshino, K. & Nishimura, S. Design, synthesis and evaluation of novel azasugar-based MMP/ADAM inhibitors. *Biorg. Med. Chem. Lett.* **13**, 2741–2744 (2003).
28. Attolino, E. *et al.* Structure-based approach to nanomolar, water soluble matrix metalloproteinases inhibitors (MMPi). *Eur. J. Med. Chem.* **45**, 5919–5925 (2010).
29. Cuffaro, D. *et al.* Matrix metalloproteinase-12 inhibitors: synthesis, structure-activity relationships and intestinal absorption of novel sugar-based biphenylsulfonamide carboxylates. *Bioorg. Med. Chem.* **26**, 5804–5815 (2018).
30. Calderone, V. *et al.* A high-affinity carbohydrate-containing inhibitor of matrix metalloproteinases. *Chem. Med. Chem.* **1**, 598–601 (2006).
31. Gerhardt, S. *et al.* Crystal structures of human ADAMTS-1 reveal a conserved catalytic domain and a disintegrin-like domain with a fold homologous to cysteine-rich domains. *J. Mol. Biol.* **373**, 891–902 (2007).
32. Akiyama, M., Takeda, S., Kokame, K., Takagi, J. & Miyata, T. Crystal structures of the noncatalytic domains of ADAMTS13 reveal multiple discontinuous exosites for von Willebrand factor. *Proc. Natl. Acad. Sci. U. S. A.* **106**, 19274–19279 (2009).
33. Petri, A. *et al.* Crystal structure and substrate-induced activation of ADAMTS13. *Nat. Commun.* **10**, 3781 (2019).
34. Wei, P. *et al.* Protein engineering and properties of human metalloproteinase and thrombospondin 1. *Biochem. Biophys. Res. Commun.* **293**, 478–488 (2002).
35. Kashiwagi, M. *et al.* Altered proteolytic activities of ADAMTS-4 expressed by C-terminal processing. *J. Biol. Chem.* **279**, 10109–10119 (2004).
36. Somerville, R. P. T. *et al.* Characterization of ADAMTS-9 and ADAMTS-20 as a distinct ADAMTS subfamily related to *Caenorhabditis elegans* GON-1. *J. Biol. Chem.* **278**, 9503–9513 (2003).
37. Ai, J., Smith, P., Wang, S., Zhang, P. & Zheng, X. L. The proximal carboxyterminal domains of ADAMTS13 determine substrate specificity and are all required for cleavage of von Willebrand factor. *J. Biol. Chem.* **280**, 29428–29434 (2005).
38. Gao, W., Anderson, P. J., Majerus, E. M., Tuley, E. A. & Sadler, J. E. Exosite interactions contribute to tension-induced cleavage of von Willebrand factor by the antithrombotic ADAMTS13 metalloprotease. *Proc. Natl. Acad. Sci. U. S. A.* **103**, 19099–19104 (2006).
39. de Groot, R., Bardhan, A., Ramroop, N., Lane, D. A. & Crawley, J. T. Essential role of the disintegrinlike domain in ADAMTS13 function. *Blood* **113**, 5609–5616 (2009).
40. Troeberg, L. *et al.* The C-terminal domains of ADAMTS-4 and ADAMTS-5 promote association with N-TIMP-3. *Matrix Biol.* **28**, 463–469 (2009).
41. Kuno, K. & Matsushima, K. ADAMTS-1 protein anchors at the extracellular matrix through the thrombospondin type I motifs and its spacing region. *J. Biol. Chem.* **273**, 13912–13917 (1998).
42. Knight, C. G. Active-site titration of peptidases. *Methods Enzymol.* **248**, 85–101 (1995).
43. Auld, D. S., Inglese, J. & Dahlin, J. L. Assay interference by aggregation. In *Assay Guidance Manual* (eds Markossian, S. *et al.*) (Eli Lilly & Company and the National Center for Advancing Translational Sciences, Bethesda, 2017).
44. Zanardelli, S. *et al.* ADAMTS13 substrate recognition of von Willebrand factor A2 domain. *J. Biol. Chem.* **281**, 1555–1563 (2006).
45. Santamaria, S. *et al.* Kinetic characterization of 4,4'-biphenylsulfonamides as selective non-zinc binding MMP inhibitors. *J. Enzyme Inhib. Med. Chem.* **30**, 947–954 (2015).
46. Morris, G. M. *et al.* AutoDock4 and AutoDockTools4: automated docking with selective receptor flexibility. *J. Comput. Chem.* **30**, 2785–2791 (2009).
47. Santos-Martins, D., Forli, S., Ramos, M. J. & Olson, A. J. AutoDock4Zn: an improved AutoDock force field for small-molecule docking to zinc metalloproteins. *J. Chem. Inf. Model.* **54**, 2371–2379 (2014).
48. Milella, L. *et al.* α -Glucosidase and α -amylase Inhibitors from *Arctophyllum thymifolium*. *J. Nat. Prod.* **79**, 2104–2112 (2016).
49. Dal Piaz, F. *et al.* Drug affinity responsive target stability (DARTS) identifies laurifolioside as a new clathrin heavy chain modulator. *J. Nat. Prod.* **79**, 2681–2692 (2016).
50. Bononi, G. *et al.* Discovery of long-chain salicylketoxime derivatives as monoacylglycerol lipase (MAGL) inhibitors. *Eur. J. Med. Chem.* **157**, 817–836 (2018).
51. Tuccinardi, T., Manetti, F., Schenone, S., Martinelli, A. & Botta, M. Construction and validation of a RET TK catalytic domain by homology modeling. *J. Chem. Inf. Model.* **47**, 644–655 (2007).

Acknowledgements

This work was supported by the Imperial College European Partners Fund 2018, British Heart Foundation project grant (PG/18/15/33566, PI J.A.) and by funding from University of Pisa (PRA_2018_20 “Approcci Target/Multitarget per il disegno e lo sviluppo di Small Molecules per terapie innovative” and “Fondi di Ateneo” 2019 to AR and EN).

We thank Dr. Suneel Apte (Cleveland Clinic, Ohio, USA) for kindly providing the V1-5GAG vector.

Author contributions

S.S., E.N., A.R., R.d.G., and J.A. designed the research; S.S., D.C. and F.L. performed the experiments; T.T. and L.C. performed the computational studies, F.D. performed the analysis of NMR data, S.S. and J.A. analyzed data; S.S., E.N., T.T., R.d.G. and J.A. wrote the paper. All authors reviewed the manuscript.

Competing interests

The authors declare no competing interests.

Additional information

Supplementary Information The online version contains supplementary material available at <https://doi.org/10.1038/s41598-020-80294-1>.

Correspondence and requests for materials should be addressed to S.S. or E.N.

Reprints and permissions information is available at www.nature.com/reprints.

Publisher's note Springer Nature remains neutral with regard to jurisdictional claims in published maps and institutional affiliations.



Open Access This article is licensed under a Creative Commons Attribution 4.0 International License, which permits use, sharing, adaptation, distribution and reproduction in any medium or format, as long as you give appropriate credit to the original author(s) and the source, provide a link to the Creative Commons licence, and indicate if changes were made. The images or other third party material in this article are included in the article's Creative Commons licence, unless indicated otherwise in a credit line to the material. If material is not included in the article's Creative Commons licence and your intended use is not permitted by statutory regulation or exceeds the permitted use, you will need to obtain permission directly from the copyright holder. To view a copy of this licence, visit <http://creativecommons.org/licenses/by/4.0/>.

© The Author(s) 2021